

A MID-INFRARED INDICATOR FOR TOTAL INFRARED LUMINOSITY AND STAR FORMATION RATE OF LOCAL AND HIGH-REDSHIFT GALAXIES

W. RUJOPAKARN¹, G. H. RIEKE¹, B. J. WEINER¹, M. REX¹, G. L. WALTH¹, J. S. KARTALTEPE²

Submitted to ApJ - 03/07/2011, Revised - 05/30/2011

ABSTRACT

We present a new method to use 24 μm observations to estimate the total infrared luminosity, $L(\text{TIR})$, and the star formation rate of star-forming galaxies across the redshift range $0 < z < 3$. This is accomplished by parameterizing the spectral energy distribution (SED) of a galaxy as a function of the $L(\text{TIR})$ surface density, $\Sigma_{L(\text{TIR})}$, instead of the traditional $L(\text{TIR})$. Our reformulation allows an accurate description of star-forming galaxy SEDs, including the aromatic emissions, out to redshift $z \sim 3.0$. We test the new 24 μm $L(\text{TIR})$ indicator against $L(\text{TIR})$ measured from stacked far-IR photometry at redshift $0 < z < 3$. We show that a monochromatic 24 μm observation can be used to estimate $L(\text{TIR})$ consistent with the values determined from the multi-band far-IR measurements such as those from *Herschel*, on average within 0.1-dex. This approach allows use of observed-frame 24 μm observation to determine the SFR of star-forming galaxies accurately across the currently expected peak of the star formation history of the universe. The success of this method indicates that a majority of IR-luminous star-forming galaxies in the universe are not strongly nuclear concentrated as are the local merger-induced LIRGs and ULIRGs.

Subject headings: cosmology: observation — galaxies: evolution — galaxies: high-redshift — infrared: galaxies

1. INTRODUCTION

Mid-Infrared (Mid-IR) wavelengths provide a unique window to study the evolution of galaxies across the history of the universe, particularly at redshift $1 < z < 3$ where the star formation rate (SFR) of the universe peaks (e.g., Hopkins & Beacom 2006). At redshift $z \gtrsim 0.5$ to 3, a majority of star formation took place in obscured environments and most of the UV photons from hot young stars, the signpost for star formation, are reprocessed by dust into IR emission (see e.g. Le Floc'h et al. 2005; Pérez-González et al. 2005; Dole et al. 2006; Buat et al. 2007). The optically extincted environment, especially in galaxies with IR luminosity, $L(\text{TIR})$, greater than the characteristic luminosity, L^* , poses inherent challenges for optical and UV determinations of the SFR.

There are two approaches to study the SFR using IR observations. Both involve using IR photometry as a tracer of $L(\text{TIR})$, which in turn traces the number of UV photons from short-lived massive stars and allows the SFR to be inferred (see e.g. Kennicutt 1998). The first approach is to use multi-band IR photometry covering the wavelengths of the peak of the IR emission to constrain the $L(\text{TIR})$ directly. Recent examples use the *Herschel* Space Observatory to observe star-forming galaxies at 100 – 500 μm (e.g. Elbaz et al. 2010; Rex et al. 2010). The complete characterization of the spectral peak of the dust emission provides a good measurement of $L(\text{TIR})$ and SFR. However, the sample size of this approach is compromised by requiring detection of an object in multiple bands that, towards longer wavelengths, are increasingly limited by confusion noise (e.g. Dole et al. 2004).

The second approach is to use a monochromatic IR luminosity to trace $L(\text{TIR})$ and SFR. Calzetti et al. (2007) have shown that the rest-frame 24 μm emission is well correlated with the ionizing photons that directly trace star formation, while shorter wavelengths such as 8 μm have a larger scatter due to the emission from stochastically heated aromatic molecules. Monochromatic far-IR indicators (70 μm and 160 μm) are affected by the emission from colder dust heated by old stars, which results in an increasing scatter in the SFR calibration as a function of wavelength, particularly in low-luminosity IR galaxies. Calzetti et al. (2010a) found that the correlation between 70 and 160 μm emission and SFR suffers from a scatter larger than that at 24 μm (Rieke et al. 2009; Kennicutt et al. 2009). These factors render 24 μm a particularly suitable monochromatic SFR indicator locally.

Beyond the local universe, however, the observed 24 μm band probes wavelengths in the spectral energy distribution (SED) of a galaxy that are increasingly affected by aromatic emissions (e.g. polycyclic aromatic hydrocarbons or PAH). At $z \sim 2$ the observed 24 μm band probes the strongest aromatic emission complexes at 6.2, 7.7, and 8.6 μm (e.g. Smith et al. 2007), which helps boost the 24 μm flux and thus aids detection of the galaxy at the cost of greater uncertainty in the estimation of the SFR. However, the most challenging issue at higher redshifts lies not in the intrinsic scatter, but rather that the aromatic emission in high-redshift star-forming galaxies at a given $L(\text{TIR})$ appears to be significantly stronger relative to $L(\text{TIR})$ than in their local counterparts (Rigby et al. 2008; Farrah et al. 2008; Takagi et al. 2010). A direct consequence of the apparent evolution of aromatic strength is that a mid-IR SFR indicator will overestimate $L(\text{TIR})$ and hence SFR by up to a factor of 5 – 7 if local SED templates are used for k-correction

¹ Steward Observatory, The University of Arizona, Tucson, AZ 85721; wiphu@as.arizona.edu

² National Optical Astronomy Observatory, 950 North Cherry Avenue, Tucson, AZ 85719, USA

without reconsidering the aromatic strength relative to the template $L(\text{TIR})$. This is reported as the “mid-IR excess” problem in recent *Herschel* results (Elbaz et al. 2010; Nordon et al. 2010). The evolution of the aromatic features in star-forming galaxy SEDs must be taken into account in using the mid-IR to indicate $L(\text{TIR})$ and SFR.

A motivation to use 24 μm observations to study the SFR despite the availability of the direct and accurate $L(\text{TIR})$ and SFR measurements from *Herschel* is that 24 μm observation still detect more individual galaxies and probe weaker SFR at any given redshift from $0 < z < 3$ (see Figure 4 of Elbaz et al. 2011). In addition to the the *Spitzer* 24 μm data in very deep survey fields, the large areas surveyed by *Spitzer* (e.g., SWIRE and the Boötes field) will not be fully surveyed by *Herschel* to the same depth in terms of $L(\text{TIR})$ or SFR. The wavelength is also uniquely accessible with current and future space missions such as *WISE* (2009, 3 – 25 μm) and *JWST* (~ 2017 , 0.6 – 28 μm).

Although the intrinsic scatter of the aromatic emission remains an issue, the larger systematic effect of the redshift evolution of aromatic emissions can be addressed by building on our previous result (Rujopakarn et al. 2011) that the $L(\text{TIR})$ surface density of a star-forming galaxy, $\Sigma_{L(\text{TIR})}$, serves as a good indicator of the SED. This paper demonstrates how this result can help select the appropriate SED template for star-forming galaxies beyond the local universe. We derive a new $L(\text{TIR})$ and SFR estimator using the observed 24 μm flux over the redshift range of $0 < z < 3$ and based on the Rieke et al. (2009) SED library for local galaxies.

The paper is organized as follows. Section 2 discusses the evolution of the SEDs of star-forming galaxies and the use of $\Sigma_{L(\text{TIR})}$ as a guide to select the appropriate SED for high-redshift galaxies. The derivation of the new monochromatic $L(\text{TIR})$ indicator is described in Section 3.1. We compare the new $L(\text{TIR})$ indicator with other independent measurements as a test in Section 3.2 and present the final $L(\text{TIR})$ and SFR indicator with further tests using larger samples in Section 4. Section 5 discusses the validity of rest-frame 8 – 24 μm as a tracer of $L(\text{TIR})$ and SFR, along with some further implications of our approach. Throughout this paper, we assume a ΛCDM cosmology with $\Omega_m = 0.3$, $\Omega_\Lambda = 0.7$, and $H_0 = 70 \text{ km s}^{-1} \text{Mpc}^{-1}$. We will refer to galaxies with $L(\text{TIR})$ in the range of $10^{11} - 10^{12}$ and those with $L(\text{TIR}) > 10^{12} L_\odot$ as Luminous Infrared Galaxies (LIRGs) and Ultraluminous Infrared Galaxies (ULIRGs), respectively, or collectively U/LIRGs. We followed the convention of Rieke et al. (2009) and adopt the definition of $L(\text{TIR})$ of Sanders & Mirabel (1996), which is generally consistent with $L(\text{TIR})$ obtained by integrating the SED template over 5 – 1000 μm .

2. QUANTIFYING THE IR SED EVOLUTION

In this section, we will discuss the challenges of using mid-IR observations, specifically *Spitzer* MIPS 24 μm photometry, to estimate $L(\text{TIR})$ and SFR both locally and at high redshift. Relevant issues are the determination of an overall approach for using $\Sigma_{L(\text{TIR})}$ as an indicator of a galaxy SED, and the choice of SED library. We will then apply this approach to describe appropriately the SED of galaxies at high redshift in terms of the local SED templates, which will be discussed in detail in

Section 3.

2.1. $\Sigma_{L(\text{TIR})}$ as an Indicator of SED for Star-Forming Galaxies

Until now, most estimations of the $L(\text{TIR})$ and SFR for moderate and high redshift ($z > 0.5$) galaxies using monochromatic IR photometry rely on an assumption that the SED of a star-forming galaxy does not evolve with redshift. SED templates of IR galaxies are constructed from local galaxies, which is an inhomogeneous population comprised of both normal disk star-forming galaxies and those with nuclear star-formation that appears to have been induced by galaxy interactions. The most IR-luminous galaxies found locally invariably represent interaction-induced star formation to various degrees (e.g. Veilleux et al. 2002). The consequence is that when we apply local IR-luminous SED templates to determine the SFR of high-redshift galaxies we make an implicit assumption that the high-redshift star-forming galaxies are similarly dominated by interaction-induced starbursts. The validity of this assumption becomes critical at $z > 0.5$ where the IR luminosity density of the universe is dominated by U/LIRGs in the luminosity range at which, locally, IR galaxies are virtually all dominated by sub-kpc nuclear regions in interacting galaxy systems.

Observations have shown that actively star-forming galaxies at high redshift are different from their local counterparts in at least three major aspects. First, the IR SEDs at high-redshift exhibit colder dust temperatures, T_d , than local galaxies at fixed $L(\text{TIR})$ (Pope et al. 2006; Symeonidis et al. 2009; Muzzin et al. 2010). In other words, these galaxies have dust temperatures consistent with local galaxies with lower $L(\text{TIR})$.

Second is that the sizes of the star-forming regions in IR galaxies at high-redshift are substantially larger than those of local galaxies at fixed $L(\text{TIR})$. Rujopakarn et al. (2011) found that IR-emitting galaxies of all luminosities at intermediate and high redshift have similar physical IR-emitting size, mostly on the order of 4 – 10 kpc, similar to local normal moderate-luminosity star-forming galaxies. By contrast, the local U/LIRGs, from which the SED templates for their corresponding luminosity are constructed, are significantly smaller with diameters on the sub-kpc scale (see Figure 3 of Rujopakarn et al. 2011). The extended size of luminous star-forming galaxies at high redshift implies a structure similar to that of local normal star-forming galaxies and differing from local U/LIRGs despite their luminosity in the U/LIRG range. This common structure is recognized in recent literature as the “main sequence” of star-forming galaxies (Noeske et al. 2007; Genzel et al. 2010; Tacconi et al. 2010; Narayanan et al. 2010; Daddi et al. 2010; Elbaz et al. 2010, 2011), where star-formation occurs at a relatively steady rate rather than in bursts, and in disks or clumps, rather than in merger nuclei. In its simplest form, this picture suggests that these galaxies differ among themselves (and from local lower luminosity star-forming galaxies) primarily in the SFR surface density, Σ_{SFR} , and hence in IR luminosity surface density, $\Sigma_{L(\text{TIR})}$.

Chakrabarti & McKee (2005) modeled the radiative transfer in centrally heated dusty sources and found a general relation among the luminosity-to-mass ratio, the surface density, and the shape of the SED. They pre-

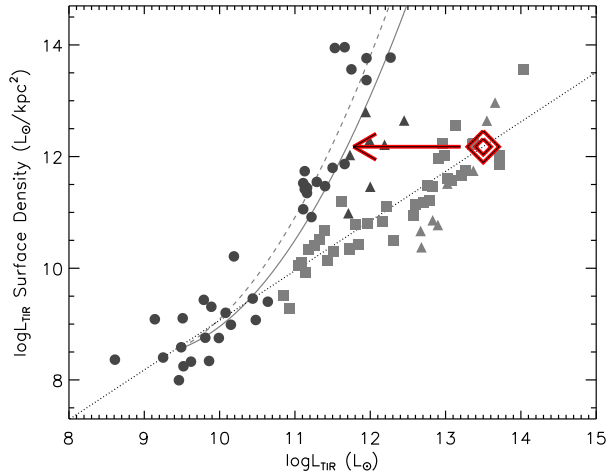


FIG. 1.— The relationships of the $L(\text{TIR})$ surface density, $\Sigma_{L(\text{TIR})}$, and $L(\text{TIR})$ differ for local U/LIRGs (circles), from which we construct the SED templates for IR galaxies, and the U/LIRGs beyond the local universe (grey squares). Upward triangles represent lower limits for both the local and high-redshift galaxies whose $\Sigma_{L(\text{TIR})}$ is derived from CO size measurements that could be systematically larger than the rest of the sample based on radio continuum measurement (Rujopakarn et al. 2011). The dotted line and the dashed line are the fits for high-redshift and local galaxies (ignoring CO lower limits), respectively. Rujopakarn et al. (2011) show that galaxy SED characteristics are indicated by $\Sigma_{L(\text{TIR})}$. This allows one to describe high-redshift galaxy SEDs with appropriate local SED templates. For example, a high-redshift galaxy with $L(\text{TIR})$ of $10^{13.5} L_{\odot}$ will have aromatic emissions and absorption features consistent with a local galaxy with the same $\Sigma_{L(\text{TIR})}$, indicated by an arrow, in this case a local galaxy with $L(\text{TIR})$ of $\sim 10^{11.5} L_{\odot}$. The method to “map” local SED templates to high-redshift galaxies is described in detail in Section 3.1. The solid line is a local fit yielding the final $L(\text{TIR})$ calibrated to the FIR observations from BLAST and *Herschel* (see Section 4.1).

dict that the behavior of SED templates for local galaxies might not extend to high redshift. Extended sizes and colder SEDs were shown to be connected through a T_d - $\Sigma_{L(\text{TIR})}$ relation explored by Chanial et al. (2007), who theoretically described the IR-emitting region of a star-forming galaxy as an isothermal cloud optically thick to optical wavelengths and optically thin in the IR. Chanial et al. (2007) also show that $L(\text{TIR})$, T_d , and the extent of the IR-emitting region are related by a fundamental plane, of which the $L(\text{TIR})$ - T_d relation (e.g. Soifer et al. 1987) is one manifestation.

Third is the aforementioned evolution of the strength of the aromatic features, which grow stronger at high redshifts at a fixed $L(\text{TIR})$. Quantitatively, for instance, Rigby et al. (2008) found a galaxy with $L(\text{TIR})$ of $10^{11.9} L_{\odot}$ at $z = 2.5$ to exhibit aromatic emission features consistent with a local galaxy with an order of magnitude lower $L(\text{TIR})$. The appropriate description of aromatic feature strength evolution is crucial because the overestimation of the resulting $L(\text{TIR})$ would otherwise exceed even the uncertainties due to intrinsic scatter (~ 0.3 -dex; Calzetti et al. 2007) especially where the aromatic complexes redshift into $24 \mu\text{m}$ band. In Rujopakarn et al. (2011), we have demonstrated that the underlying parameter explaining the apparent evolution is the $\Sigma_{L(\text{TIR})}$.

In Figure 1, adapted from Figure 4 of Rujopakarn et al.

(2011), we show $\Sigma_{L(\text{TIR})}$ as a function of $L(\text{TIR})$ along with trend lines describing the relationship in each population, one for local galaxies with $L(\text{TIR})$ above $10^{11} L_{\odot}$ and another for high-redshift galaxies. The surface area of the IR-emitting region used to estimate $\Sigma_{L(\text{TIR})}$ is measured by radio continuum (e.g., 1.4 GHz), Paschen- α , or $24 \mu\text{m}$ observations such that they reflect the size of the star-forming regions but are insensitive to the contribution from old stellar populations. The main sequence can be drawn in this figure from the local normal star-forming galaxies (non-U/LIRGs) onto the high-redshift star-forming galaxies. Both local and high-redshift trend lines agree at low luminosity, but the trend that includes local U/LIRGs diverges from the main sequence at $L(\text{TIR}) \sim 10^{11} L_{\odot}$ where the local galaxy sample starts to be drawn from the interaction-dominated U/LIRGs populations. Drawing a horizontal line at fixed $\Sigma_{L(\text{TIR})}$ in Figure 1 for the Rigby et al. (2008) example, we expect the galaxy on the main sequence with $L(\text{TIR})$ of $10^{11.9} L_{\odot}$ to have spectral features consistent with a galaxy on the local sequence with $L(\text{TIR})$ of $\sim 10^{10.9} L_{\odot}$, which agrees with the observed aromatic features. Rujopakarn et al. (2011) further demonstrated the use of $\Sigma_{L(\text{TIR})}$ to predict SED behavior by predicting the $24 \mu\text{m}$ -to-1.4 GHz flux ratios and matching the observed stacked aromatic spectrum of high-redshift ULIRGs to a local SED template.

We therefore adopt the assumption that $\Sigma_{L(\text{TIR})}$ is the dominant parameter controlling the average SED. Given the large range of $\Sigma_{L(\text{TIR})}$ represented in both the main sequence and the local U/LIRGs, it is then possible to choose an appropriate SED to represent high-redshift U/LIRGs. Apart from the Chanial et al. (2007) fundamental relationship, this approach is also physically motivated in that the aromatic emission emerges from the outer surfaces of the photodissociation regions (PDRs; e.g. Tielens 2008), so the surface density of the star formation rate in a galaxy is among the controlling factors for the aromatic-emitting surface of a galaxy.

2.2. Selection of the Local Reference for the Galaxy SED

The most widely used local SED libraries are those of Chary & Elbaz (2001), Dale & Helou (2002), and Rieke et al. (2009). The former two libraries were based on spectra taken by *ISO* that do not fully span the $6 - 24 \mu\text{m}$ wavelength range that the $24 \mu\text{m}$ band probes at redshift $z = 3 - 0$. The recent infrared spectrograph (IRS) observations from *Spitzer*, covering $5.2 - 38 \mu\text{m}$, show that the Chary & Elbaz (2001) SED templates (hereafter, CE01) have suppressed aromatic features at very high luminosity and do not sufficiently take into account the strong silicate absorption features at $\sim 10 \mu\text{m}$, resulting in weaker aromatic bands but stronger overall emission in the mid-IR inconsistent with actual galaxy SEDs (Armstrong et al. 2007; Rieke et al. 2009). The Dale & Helou (2002) SED library is optimized to describe moderately-luminous local star-forming galaxies with $L(\text{TIR}) < 10^{11} L_{\odot}$ and hence the lack of silicate absorption becomes more evident, especially at higher $L(\text{TIR})$ with larger extinction. We therefore adopt the Rieke et al. (2009) SED library (hereafter, R09) for a local SED reference.

Rieke et al. (2009) constructed SED templates separately for normal star-forming galaxies (sub-LIRG) and those in U/LIRG range in order for the final SED library to cover $L(\text{TIR})$ of $10^{9.75}$ to $10^{13.00} L_{\odot}$. The U/LIRGs SED templates were constructed from a sample of 11 local LIRGs and ULIRGs with high quality *Spitzer* IRS spectra as well as photometric data covering optical to radio wavelengths (see Figure 1, 2, and 3 of Rieke et al. (2009)). These U/LIRGs were chosen such that their IR emission is dominated by star-forming activity. Construction of the SED library is done in two steps. First, these 11 galaxies were used as a basis to assemble 11 archetypal SED templates spanning $0.4 \mu\text{m}$ to 30 cm wavelength. Their IRS spectra ($5 - 38 \mu\text{m}$) were joined to the photospheric emission and far-IR dust emission components in a series of tests to ensure both spectral continuity and appropriate flux calibration. Second, these archetypal templates are combined with different weights to produce the final averaged SED templates. The template weights are optimized by matching synthesized IR colors from the combined template to IR colors of observed galaxies with known $L(\text{TIR})$ from the *IRAS* RBGS (Sanders et al. 2003). The R09 library construction was extended to star-forming galaxies with sub-LIRG $L(\text{TIR})$ by combining the Dale & Helou (2002) SED library with the recent mid-IR spectral library based on IRS observations from Smith et al. (2007) using the same IR color fitting technique as the U/LIRGs template construction. The use of IR color to help guide the combination of archetypal templates (i.e. fitting $25/8 \mu\text{m}$, $25/12 \mu\text{m}$, and $60/25 \mu\text{m}$ colors simultaneously) helps ensure that the final templates represent the average property of real galaxies even though they are constructed from a limited sample. The R09 SED library construction is described in detail in the Appendix of Rieke et al. (2009).

3. A MID-IR ESTIMATOR FOR $L(\text{TIR})$ AT $0 < z < 3$

The construction of a $24 \mu\text{m}$ SFR indicator has two steps: (1) to construct an $L(\text{TIR})$ estimator using $24 \mu\text{m}$ photometry, and then (2) to derive a relationship between $L(\text{TIR})$ and SFR. We discuss construction of the $L(\text{TIR})$ estimator in Section 3.1 and test it by comparing our $L(\text{TIR})$ estimates to $L(\text{TIR})$ derived from other independent measurements in Section 3.2. The test is then used to refine our $L(\text{TIR})$ indicator, which we provide in final form in Section 4 along with the relationship between $L(\text{TIR})$ and SFR.

3.1. Construction of a Mid-IR $L(\text{TIR})$ Indicator

The process of calculating the $L(\text{TIR})$ typically involves finding the best-match SED for a set of observed fluxes at a given redshift and then integrating the SED (e.g. Pérez-González et al. 2005; Le Floc'h et al. 2005; Magnelli et al. 2009). For monochromatic indicators, this means fitting an SED using a single data point, which leaves significant room for uncertainties. Rieke et al. (2009) circumvent this process by first assigning a value of $L(\text{TIR})$ to each SED template and then determining their corresponding SFR as well as the monochromatic luminosity through the desired filter. For the $24 \mu\text{m}$ band, in particular, the assignment

TABLE 1
STRETCHING FACTORS AND $L(\text{TIR})_{\text{new}}$ ASSOCIATED TO
RIEKE ET AL. (2009) SED TEMPLATES

$\log L(\text{TIR})_{\text{old}}^{\dagger}$	$\log S_i$	$\log L(\text{TIR})_{\text{new}}$	$\log S_i^*$	$\log L(\text{TIR})_{\text{new}}^*$
9.75	-0.047	9.70	-0.128	9.62
10.00	0.026	10.03	-0.127	9.87
10.25	0.177	10.43	-0.049	10.20
10.50	0.400	10.90	0.098	10.60
10.75	0.701	11.45	0.321	11.07
11.00	1.074	12.07	0.614	11.61
11.25	1.526	12.78	0.982	12.23
11.50	2.049	13.55	1.420	12.92
11.75	2.651	14.40	1.934	13.68
12.00	3.325	15.33	2.518	14.52

NOTE. — Col 1: Original $L(\text{TIR})$ associated to each of the Rieke et al. (2009) SED templates; Col 2: stretch factors from the formal fit to the $L(\text{TIR})$ - $\Sigma_{L(\text{TIR})}$ relationship of local galaxies (Section 3.1); Col 3: resulting $L(\text{TIR})_{\text{new}}$ associated to SED template shape from the formal fit; Col 4: stretch factors from the final $L(\text{TIR})$ - $\Sigma_{L(\text{TIR})}$ parameterization calibrated to FIR observations (Section 4.1); Col 5: resulting $L(\text{TIR})_{\text{new}}$ from the final parameterization.

[†] The Rieke et al. (2009) SED templates with $L(\text{TIR})_{\text{old}} > 10^{12} L_{\odot}$ are omitted because their $L(\text{TIR})_{\text{new}}$ are higher than luminosities of observed galaxies. These SED template shapes are thus unlikely to represent real galaxies at high redshift.

of the $24 \mu\text{m}$ luminosity of a template follows the ratio of $L(24 \mu\text{m})$ -to- $L(\text{TIR})$ based on the local *IRAS* data (see Fig. 8, Fig. 15, and formula A6 of Rieke et al. 2009). Once each template has an associated $24 \mu\text{m}$ luminosity, it is possible to calculate the k-corrections and subsequently the expected monochromatic flux for each template as a function of redshift. For $L_{\nu} \propto \nu f_{\nu}$, the k-correction, $K_{\text{corr}}(z)$, and the flux, $f_{\nu}(24 \mu\text{m})$, are related by

$$K_{\text{corr}}(z) = (1+z) \frac{f_{\nu}(\nu = (1+z)\nu_{\text{obs}})}{f_{\nu}(24 \mu\text{m})} \quad (1)$$

$$4\pi D_L^2 f_{\nu, \text{obs}} = \frac{L_{\nu, \text{rest}}(24 \mu\text{m})}{\nu_{24}} K_{\text{corr}}(z) \quad (2)$$

where D_L is the luminosity distance for an object at redshift z . The $4\pi D_L^2 f_{24, \text{obs}}$ for this equation has the unit of Jy cm^2 . The relationship between the observed monochromatic flux from each template and the template's monochromatic luminosity at a given redshift is approximately linear, which allows for a linear fit to be performed at each redshift (i.e. for a redshift grid) to determine a set of coefficients that convert the observed flux at a given redshift to the luminosity or any desired quantity associated with the template (i.e. $L(\text{TIR})$ or SFR). For example, a relationship between $L(\text{TIR})$ and the observed $24 \mu\text{m}$ flux, $f_{24, \text{obs}}$, would have the form

$$\log L(\text{TIR})_{\text{old}} = A(z) + B(z) [\log(4\pi D_L^2 f_{24, \text{obs}}) - C], \quad (3)$$

where $A(z)$ and $B(z)$ are the intercept and the slope from the linear fit, respectively, C is a zero-point to reduce covariance in the fit parameters, and $L(\text{TIR})_{\text{old}}$ refers to the $L(\text{TIR})$ associated to each of the R09 SED templates. Rieke et al. (2009) use this method to tabulate the coefficients to convert the monochromatic fluxes in various bands to the SFR of galaxies.

Because of the evolution of the IR SEDs, a different approach is needed to derive suitable templates for them. Following Rujopakarn et al. (2011), an appropriate choice of SED to use for k-correction beyond the local universe is the one corresponding to the same $\Sigma_{L(\text{TIR})}$ locally. This is equivalent to increasing the $L(\text{TIR})$ associated with each of the R09 SED templates by a factor determined by the ratio of luminosities with equal $\Sigma_{L(\text{TIR})}$ on the local U/LIRGs trend to those on the main sequence. We will refer to this ratio as the *stretching factor*, S_i , for each SED template. Note from Figure 1 that S_i is nearly negligible at $L(\text{TIR}) \sim 10^{11} L_\odot$ and reaches three orders of magnitude at $L(\text{TIR})$ of $10^{14} L_\odot$. To determine S_i quantitatively, we parameterize the relationship by fitting a 2nd-order polynomial to the local U/LIRG relation (excluding the lower limits of $\Sigma_{L(\text{TIR})}$ from CO observations) and a linear fit to the main sequence, and then take the ratio of $L(\text{TIR})$ on the main sequence fit to the R09 template $L(\text{TIR})$ at the same $\Sigma_{L(\text{TIR})}$ (see Figure 1; the S_i values are tabulated in Table 1). Since we effectively increase the luminosity of each template by a factor of S_i , the observed flux will also be increased by the same factor. Equation 3 can thus be rewritten as

$$\begin{aligned} \log L(\text{TIR})_{\text{new}} &= \log [S_i L(\text{TIR})_{\text{old}}] \\ &= A'(z) + B'(z) [\log(4\pi D_L^2 S_i f_{24,\text{obs}}) - C'] \end{aligned} \quad (4)$$

The new set of coefficients, $A'(z)$, $B'(z)$, and C' that use the appropriate SED templates for main sequence star-forming galaxies at redshift $0 < z < 3$ can be determined by re-fitting equation 4. We have limited the fitting range to only encompass the “stretched” luminosity of $\log L(\text{TIR})_{\text{new}} < 14$. This is because the S_i are very large at high luminosity and the stretched luminosities are well above the luminosity range occupied by real galaxies (the $10^{14} L_\odot$ cut off is chosen because we expect this to be at or beyond the upper luminosity limit of star-forming galaxies). For a given template, the shape as a function of redshift remains the same. The effect of the S_i is to change the spacing between templates. The relationship between luminosity and observed flux remains well approximated as linear, with residuals < 0.05 dex.

The fitting coefficients, $A'(z)$ and $B'(z)$, to relate the observed *Spitzer* 24 μm flux to $L(\text{TIR})$ as a function of redshift, are shown in Figure 2 (as dotted lines). The zero-point, C' , for the formula is 45. Thus the relation is

$$\log L(\text{TIR})_{\text{new}} = A'(z) + B'(z) [\log(4\pi D_L^2 f_{24,\text{obs}}) - 45], \quad (5)$$

As is the case for Rieke et al. (2009), the feature in $A'(z)$ and $B'(z)$ at $z \sim 1.4$ is due to silicate absorption, which depends on template luminosity.

3.2. Comparison of $L(\text{TIR})$ to Far-IR $L(\text{TIR})$ Measurements

We test our $L(\text{TIR})$ indicator in two steps. In this section, we apply it to small samples of galaxies with accurately measured $L(\text{TIR})$ from far-IR bands covering the spectral peak of dust emission (e.g. 200 – 500 μm). Using the result from this step, we make fine adjustments to the indicator in Section 4.1 and perform a series of blind tests on large samples with more limited far-IR

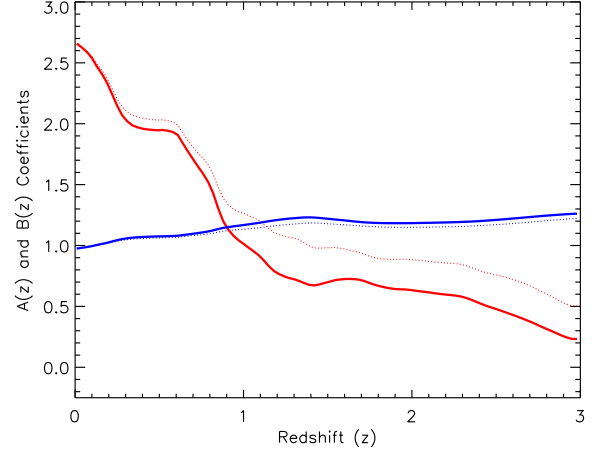


FIG. 2.— The coefficients of the fits for a relationship between the observed *Spitzer* 24 μm flux and the total IR luminosity (Equation 5) as a function of redshift. The coefficients $A'(z)$ and $B'(z)$ are shown by the dotted red and blue lines. The red and blue solid lines represent the final coefficients $A^*(z)$ and $B^*(z)$ resulting from a fit calibrated to the FIR $L(\text{TIR})$ measurements. The latter set of coefficients are tabulated in Table 2.

photometric coverage (e.g. 24 – 160 μm) to investigate the performance of the indicator.

For the first step, we compared the $L(\text{TIR})$ estimated from our method with those derived from the integration of SEDs fitted to the FIR observations from *Herschel* as well as the Balloon-borne Large Aperture Submillimeter Telescope (BLAST; e.g. Pascale et al. 2008; Dye et al. 2009; Eales et al. 2009). We also compared our $L(\text{TIR})$ to those estimated using the CE01 and the original R09 SED libraries.

The *Herschel* data used for this test were taken from the *Herschel* Lensing Survey (HLS; Egami et al. 2010). The sample consists of 19 galaxies located behind the Bullet Cluster at redshifts $0.4 < z < 3.2$ (Rex et al. 2010). These sources are detected in at least two *Herschel* bands (at 100–500 μm) and many are also observed in LABOCA 870 micron and AzTEC 1.1 mm maps of the field (Wilson et al. 2008; Johansson et al. 2010). These measurements tightly constrain the peak of the FIR SED and therefore provide accurate estimates of $L(\text{TIR})$. We have excluded one object from this sample, HLS18, because its large lensing magnification ($54\times$) is not well constrained due to nearby objects (Rex et al. 2010).

The BLAST data we used are a subset of 27 galaxies from the photometric catalog of BLAST sources located in the Chandra Deep Field South presented in Dye et al. (2009) that have spectroscopic redshift measurements (Eales et al. 2009). The BLAST photometry was originally calibrated based on observations of the red supergiant star VY CMa (Truch et al. 2009). Recent SPIRE FTS observations of this calibration source reveal significant emission lines within the BLAST bandpasses (Royer et al. 2010). Convoluting the observed spectrum for VY CMa with the BLAST filter transmission curves indicates excess flux at the level of 0.06–dex compared with the originally assumed blackbody. For this work the BLAST fluxes have therefore been rescaled by this factor to accurately match the SPIRE measurements. The galaxies in this sample have photometric measurements in at least two of the BLAST bands (at 250 – 500 μm)

which are augmented in most cases by *Spitzer* 24, 70 and 160 micron data for SED fitting. The BLAST data are ultimately limited by source confusion at submillimeter wavelengths; the catalog is therefore dominated by main sequence galaxies at redshift $z < 0.5$. All of the higher redshift galaxies are contaminated by AGN and are excluded based on their classification by Eales et al. (2009).

Figure 3 compares $L(\text{TIR})$ estimated from this work with that derived from the HLS and BLAST data, as well as the same comparison for $L(\text{TIR})$ based on the CE01 and R09 SED libraries. The figure demonstrates the “mid-IR excess” by which the 24 μm monochromatic indicator over-estimates $L(\text{TIR})$ compared with that measured by integrating the SED fitted to far-IR data. The mid-IR excess is significant for the monochromatic 24 μm -derived $L(\text{TIR})$ using both the CE01 and the original R09 SED libraries. However, the excess is alleviated by using our adjusted indicator and the resulting monochromatic 24 μm -derived $L(\text{TIR})$ agrees well with the far-IR observations.

It appears from Figure 3 that the CE01 SED library is less prone to overestimating $L(\text{TIR})$ for high-redshift galaxies compared to the R09 library. A careful comparison of the two template sets has, however, shown that the omission of silicate absorption features in the CE01 SED templates results in an overestimation of aromatic-region flux in the local SED templates that coincidentally helps partially compensate the PAH-region flux evolution at high redshift. The R09 templates correctly include the silicate absorption locally, and hence suffer a larger overestimation of $L(\text{TIR})$ at intermediate and high redshift (see the appendix of Rieke et al. (2009) for a detailed discussion of uncertainties in high-redshift behavior of the SED templates). We have now shown that the R09 templates can be used to extrapolate for $L(\text{TIR})$ accurately from monochromatic 24 μm observations given an appropriate choice of SED template based on the $\Sigma_{L(\text{TIR})}$.

4. FINAL APPROACH TO DETERMINING $L(\text{TIR})$ AND SFR

In this section we discuss a slightly modified calibration of our template selection to provide the final indicator along with the relationship between $L(\text{TIR})$ and SFR. The final indicator is then tested against large samples of star-forming galaxies from cosmological surveys to verify its integrity over $0 < z < 3$.

4.1. An Alternate Calibration Based on a Modified Parameterization to the Local $L(\text{TIR})$ - $\Sigma_{L(\text{TIR})}$ Relationship

Figure 3 hints at a small (< 0.2 -dex) yet systematic of underestimation of $L(\text{TIR})$ at high luminosity, especially at $L(\text{TIR}) > 10^{12} L_{\odot}$. A possible cause of the underestimation is that there are other underlying higher-order parameters that affect the SED shape at high luminosity other than our simple assumption that the SED shape is indicated by $\Sigma_{L(\text{TIR})}$. This necessitates future explorations of the SED dependence on a broader range of parameters, such as redshift, luminosity, metallicity, and environment. A second possibility leading to the underestimation could be the uncertainties in the local fit of the $L(\text{TIR})$ - $\Sigma_{L(\text{TIR})}$ relationship that is constrained by a sample of 44 local galaxies, only 25 of which are in the U/LIRG luminosity range. A larger sample of local galaxies in the U/LIRGs range would be ideal, but

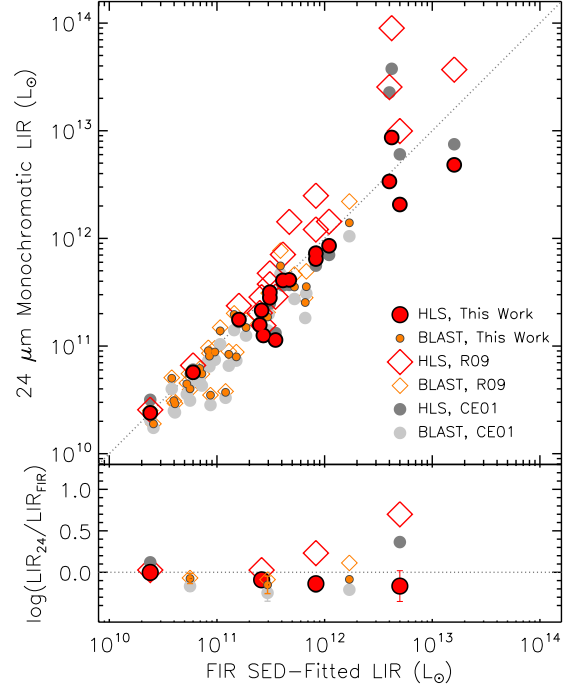


FIG. 3.— Comparison of $L(\text{TIR})$ derived from this work and the SED libraries of Chary & Elbaz (2001) and Rieke et al. (2009), labeled as CE01 and R09, respectively, to the $L(\text{TIR})$ measured by integrating the far-IR multi-band photometry from *Herschel* Space Observatory and the Balloon-borne Large Aperture Submillimeter Telescope (BLAST). The mid-IR excess problem (Section 3.2) is shown to be alleviated by the new $L(\text{TIR})$ indicator. Our 24 μm -based $L(\text{TIR})$ is derived from the local $L(\text{TIR})$ - Σ_{SFR} relation fit that excludes CO lower-limit measurements (Fig. 1). Note that in the bottom plot, the averaged data point is shown at the median luminosity in the corresponding bin. At high- $L(\text{TIR})$, this indicator exhibits a slight underestimation of $L(\text{TIR})$ compared to the FIR measurements. Nevertheless, our monochromatic estimate of $L(\text{TIR})$ is consistent with the FIR $L(\text{TIR})$ measurements within 0.2-dex on average. This underestimation could be a result of the uncertainties in the parameterization of the local $L(\text{TIR})$ - Σ_{SFR} relationship as well as the possibility of higher-order underlying parameters other than the $\Sigma_{L(\text{TIR})}$ that could affect the shape of high-redshift galaxy SEDs. We provide a separate relationship based on the same $\Sigma_{L(\text{TIR})}$ method that improves agreement of our monochromatic $L(\text{TIR})$ estimates and the FIR $L(\text{TIR})$ measurements as shown in Fig. 4.

the sample size is limited by the number of known local U/LIRGs that do not harbor significant AGN activity and have good size measurements.

In light of the uncertainties of the local $L(\text{TIR})$ - $\Sigma_{L(\text{TIR})}$ relationship (dashed line in Figure 1), it is possible to modify the parameterization of this relationship by calibrating the monochromatic $L(\text{TIR})$ to the FIR $L(\text{TIR})$ observations from *Herschel* and BLAST. This is done by optimizing a 3rd-order polynomial describing the local $L(\text{TIR})$ - Σ_{SFR} relationship to minimize the differences between the resulting $L(\text{TIR})$ estimated by our indicator and the $L(\text{TIR})$ based on FIR measurements. From this parameterization, we calculate new stretching factors, S_i^* , tabulated in Table 1, which results in the final coefficients for equation 5, $A^*(z)$ and $B^*(z)$, tabulated in Table 2 and shown in Figure 2 in comparison with $A'(z)$ and $B'(z)$ derived in Section 3.1. The modi-

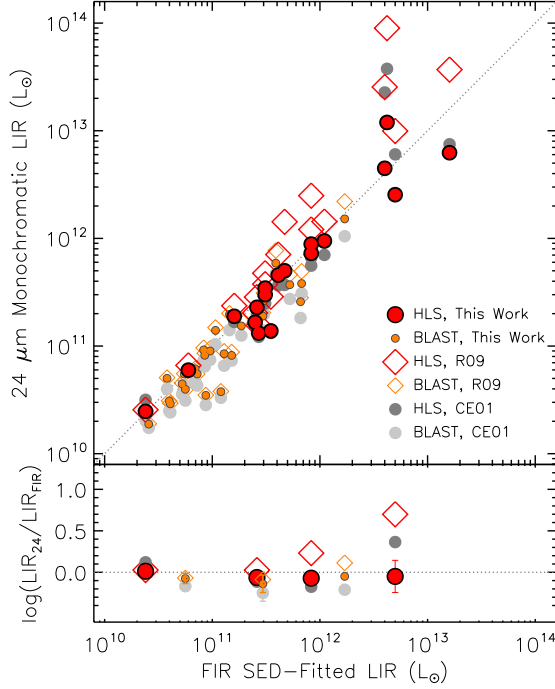


FIG. 4.— $L(\text{TIR})$ estimated from $24\ \mu\text{m}$ observations using the $\Sigma_{L(\text{TIR})}$ as an indicator of SED shape and a modification of the local $L(\text{TIR})$ - $\Sigma_{L(\text{TIR})}$ relation to calibrate the final $L(\text{TIR})$ to the FIR $L(\text{TIR})$ measurements. The symbols are the same as in Fig. 3. This relationship allows one to estimate $L(\text{TIR})$ and SFR consistent with the FIR measurements (e.g. *Herschel* and BLAST) on average within 0.1–dex using monochromatic $24\ \mu\text{m}$ observations. The final $L(\text{TIR})$ estimates agree with the FIR $L(\text{TIR})$ measurements on average within 0.1–dex (Figure 4).

With the final parameterization, we also tabulated the luminosity of the appropriate R09 SED template that should be used to describe star-forming galaxies given the $24\ \mu\text{m}$ observed flux and redshift in Table 3. Even at the bright-end of the flux range at high redshift (e.g. $f_{24} = 3.0\ \text{mJy}$ at $z = 3.0$, which corresponds to $L(\text{TIR})$ of $10^{14.6}\ L_{\odot}$), the appropriate R09 template for such galaxy is that of a local ULIRG with $L(\text{TIR})$ of $10^{12.0}\ L_{\odot}$. In fact, it is evident from the table that most IR-luminous star-forming galaxies at $0 < z < 3$ exhibit spectral characteristics of local galaxies with $L(\text{TIR})$ in the range of $10^{11} - 5 \times 10^{11}\ L_{\odot}$.

4.2. Testing the Final $L(\text{TIR})$ Indicator with Samples from Large Cosmological Surveys

There are two aspects of the test required to establish the reliability of our $L(\text{TIR})$ indicator in real-life usage, based on estimating $L(\text{TIR})$ in blind samples of galaxies from cosmological surveys. First is to quantify the scatter of the resulting $L(\text{TIR})$ compared to $L(\text{TIR})$ derived

TABLE 2
COEFFICIENTS OF
THE FINAL FITS FOR
THE RELATION
BETWEEN *Spitzer* $24\ \mu\text{m}$ FLUX AND THE
 $L(\text{TIR})$

z	$A^*(z)$	$B^*(z)$
0.0	2.669	0.973
0.2	2.303	1.026
0.4	1.960	1.070
0.6	1.915	1.080
0.8	1.490	1.118
1.0	1.014	1.168
1.2	0.775	1.209
1.4	0.675	1.231
1.6	0.725	1.206
1.8	0.669	1.185
2.0	0.633	1.184
2.2	0.597	1.189
2.4	0.527	1.200
2.6	0.429	1.222
2.8	0.315	1.245
3.0	0.232	1.263

NOTE. — $A^*(z)$ and $B^*(z)$ are the coefficients for equation 5 derived from the final parameterization of the relationship calibrated to FIR observations (solid line in Fig. 1). See details in Section 3.1 and 4.1.

from multi-band SED fitting. Second, and more importantly, is to verify that the indicator accurately describes the SED features of galaxies over $0 < z < 3$, i.e. that the mid-IR excess problem has been resolved. We conclude from the tests in this section that our $L(\text{TIR})$ indicator accurately estimates $L(\text{TIR})$ within 0.1–dex on average compared to $L(\text{TIR})$ determined from SED-fitting and with scatter of less than 0.26–dex.

We adopt three samples for these tests: (1) the $70\ \mu\text{m}$ -selected COSMOS sample ($n = 751$) from Kartaltepe et al. (2010); (2) the stacked $70\ \mu\text{m}$ and $160\ \mu\text{m}$ photometry of $24\ \mu\text{m}$ -selected sample from Lee et al. (2010) in COSMOS ($n > 35,000$); and (3) the stacked $24\ \mu\text{m}$, $70\ \mu\text{m}$, $160\ \mu\text{m}$, $1.4\ \text{GHz}$, and $610\ \text{MHz}$ observations of a NIR-selected sample ($n = 3,172$) from the Extended Chandra Deep Field-South survey (ECDFS) (Bourne et al. 2011). Unlike the *Herschel* and BLAST samples, these $L(\text{TIR})$ estimates rely on extrapolating a fitted-SED to the dust emission peak. The goal of this section is thus not to re-calibrate our indicator, but to test it on a large sample across a broad redshift range.

To quantify the scatter, we compare our final $L(\text{TIR})$ calibration to the $L(\text{TIR})$ estimates from the $70\ \mu\text{m}$ -selected COSMOS sample (Kartaltepe et al. 2010); the entire sample contains 1503 galaxies at $0.0 < z < 3.5$. Kartaltepe et al. (2010) estimated $L(\text{TIR})$ by fitting IR photometry from *Spitzer* at the 8 , 24 , 70 , and $160\ \mu\text{m}$ bands to an extensive collection of SED libraries and selected the best fit via χ^2 minimization among the Chary & Elbaz (2001), Dale & Helou (2002), Lagache et al. (2003), and Siebenmorgen & Krügel (2007) templates. For our com-

TABLE 3
THE LUMINOSITY OF THE APPROPRIATE RIEKE ET AL. (2009) SED
TEMPLATE TO DESCRIBE SED OF A STAR-FORMING GALAXY FOR A GIVEN
24 μ m FLUX AND REDSHIFT

f_{24} (mJy)	0.10	0.50	0.75	1.00	Redshift (z)					
					1.25	1.50	1.75	2.00	2.50	3.00
0.02	...	9.9	10.2	10.3	10.6	10.7	10.6	10.7	10.9	11.1
0.05	...	10.2	10.5	10.6	10.8	10.9	10.9	10.9	11.1	11.3
0.1	...	10.4	10.6	10.8	11.0	11.1	11.1	11.1	11.2	11.4
0.2	...	10.6	10.8	11.0	11.2	11.2	11.2	11.2	11.4	11.6
0.4	9.7	10.8	11.0	11.1	11.3	11.4	11.3	11.4	11.5	11.7
0.8	9.9	10.9	11.1	11.3	11.4	11.5	11.5	11.5	11.6	11.8
1.5	10.2	11.1	11.2	11.4	11.6	11.6	11.6	11.6	11.7	11.9
3.0	10.4	11.2	11.4	11.5	11.7	11.7	11.7	11.7	11.8	12.0

NOTE. — Dots indicate that the combination of flux and redshift would yield a SED template that is outside the luminosity range of the Rieke et al. (2009) SED library. The result from the final form of the local $L(\text{TIR})-\Sigma_{L(\text{TIR})}$ relationship (4.1) is used here.

parison, we exclude sources with X-ray luminosity $> 10^{42}$ erg/s, those with radio-excess, and those exhibiting power-law SEDs in the *Spitzer* IRAC bands to minimize AGN contamination. Above $10^{12.5} L_{\odot}$, the Kartaltepe et al. (2010) sample contains very few sources that do not harbor AGN or QSO. Kartaltepe et al. (2010) show that sources with 160 μ m detections are biased toward objects with colder dust, whose $L(\text{TIR})$ may not directly correlate with SFR, and therefore we also exclude these sources. Lastly, we limit our comparison sample to those with uncertainties in SED-fitted $L(\text{TIR}) < 0.35$ dex to avoid comparing to outliers with large uncertainties in luminosity. After applying these cuts, we have 751 sources left. These sources have redshifts ranging from $z = 0.07$ to 1.81 with a mean and median redshift of 0.52 and 0.43. The luminosity of this subsample ranges from $L(\text{TIR})$ of $10^{9.5}$ to $10^{12.5} L_{\odot}$ and both mean and median $L(\text{TIR})$ of $10^{11.1}$ and $10^{11.2} L_{\odot}$, respectively.

The comparison shown in Figure 5 indicates an offset of ~ 0.05 -dex between our $L(\text{TIR})$ estimates and those of Kartaltepe et al. (2010) across the luminosity range. This offset is identical for $L(\text{TIR})$ estimates based on Rieke et al. (2009) and Chary & Elbaz (2001) at $L(\text{TIR}) < 10^{11} L_{\odot}$ and is likely due to a difference in convention of $L(\text{TIR})$ between the indicators. Apart from this offset, the estimates are consistent within 0.1-dex at $L(\text{TIR})$ of $10^{9.5} - 10^{12.5} L_{\odot}$ with an average internal scatter of 0.26-dex. Some fraction of this scatter must arise in the assignment of $L(\text{TIR})$ by Kartaltepe et al. (2010); hence, it is an upper limit relative to our $L(\text{TIR})$ estimates. In addition to estimating the scatter, the comparison with the Kartaltepe et al. (2010) sample allows us to test our $L(\text{TIR})$ estimates particularly at $z \sim 0.4$ where the 17 μ m aromatic complex redshifts into the 24 μ m band. The agreement with Kartaltepe et al. (2010) indicates that our SED assignment method adequately describes the aromatic emission strength.

Apart from testing the 24 μ m monochromatic $L(\text{TIR})$ indicator, we also use the modified local $L(\text{TIR})-\Sigma_{\text{SFR}}$ relationship to derive the $A(z)$ and $B(z)$ coefficients to estimate $L(\text{TIR})$ from the 70 μ m observed flux (e.g. *Spitzer* MIPS or *Herschel* PACS). The resulting coefficients yield monochromatic 70 μ m $L(\text{TIR})$ consistent

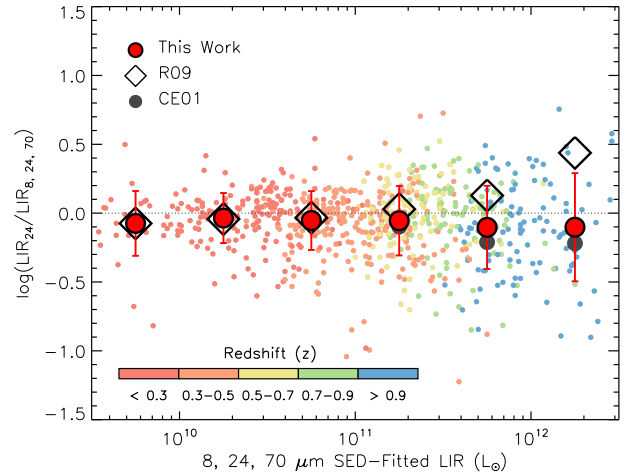


FIG. 5.— The scatter of our $L(\text{TIR})$ indicator is estimated by comparing our final calibration (Section 4.1) to those from multi-band SED fitting in the COSMOS sample (Kartaltepe et al. 2010) of 751 galaxies at redshift $0.0 < z < 1.8$. Red circles, diamonds, and grey circles represent $L(\text{TIR})$ estimates from this work, the R09, and the CE01 SED library, respectively. Color-coded points are individual galaxies. Error bars reflect the internal scatter in each luminosity bin, which is on average 0.26-dex. Apart from the systematic offset of ~ 0.05 -dex across the luminosity range, our monochromatic $L(\text{TIR})$ indicator yields results consistent within 0.1-dex of multi-band SED fitting. The agreement of $L(\text{TIR})$ at redshift $z \sim 0.4$ and $z \sim 1$ where the 17 μ m and 11 μ m aromatic emission complexes redshift into the 24 μ m band suggests that our method accurately predicts the spectral features.

with the values from the original Rieke et al. (2009) estimator at $L(\text{TIR}) < 10^{11} L_{\odot}$ and overestimate the Rieke et al. (2009) $L(\text{TIR})$ by < 0.15 -dex at higher luminosities. We do not anticipate strong evolution of the SED in the rest-frame wavelength range probed by the observed 70 μ m band at redshift $z = 0 - 3$ ($70 - 17.5 \mu$ m) because it is still in the Wien tail region of the dust blackbody emission, unlike the 24 μ m band. Thus the Rieke et al. (2009) coefficients can be used to estimate $L(\text{TIR})$ and SFR from 70 μ m flux.

The second test employs the Lee et al. (2010) sample that stacks 70 μ m and 160 μ m observations of over 35,000 galaxies selected at 24 μ m in COSMOS. The stacks were done in bins of 24 μ m flux ($0.06 < f_{24} < 3.00$ mJy)

and redshift ($0 < z < 3$). We note that although Kartaltepe et al. (2010) found that individual sources detected at $160\ \mu\text{m}$ are biased toward galaxies with cold dust as mentioned earlier, the same study also found that the stacked $160\ \mu\text{m}$ flux from galaxies not detected individually is not affected by this bias and hence the $160\ \mu\text{m}$ stacked photometry can be used reliably. Lee et al. then fit SEDs to the average $24\ \mu\text{m}$, $70\ \mu\text{m}$ and $160\ \mu\text{m}$ fluxes in each stacked bin with the same procedure as that of Kartaltepe et al. (2010) to estimate $L(\text{TIR})$, which we use to test our indicator. We have excluded bins where the fraction of X-ray sources (probably associated with AGN) exceeds 0.1 based on Figure 3 of Lee et al. (2010). For the actual $L(\text{TIR})$ calculation we use the average value of $24\ \mu\text{m}$ flux and redshift in each bin (N. Lee, 2011, private communication) to calculate the average $L(\text{TIR})$ of the bin, which can be compared with the estimates from Lee et al. (2010). The result from this test is presented in Figure 6.

Finally we used the stacking result from Bourne et al. (2011). Their sample of 3172 galaxies was selected using *Spitzer* IRAC $3.6\ \mu\text{m}$ and $4.5\ \mu\text{m}$ photometry (i.e. probing stellar mass) in ECDFS. The selection of the sample in the near-IR provides an independent sample that might reveal selection effects (if any) inherent to mid- and far-IR selections (e.g. the Lee et al. and Kartaltepe et al. samples). Bourne et al. then stacked observations of the sample in 7 redshift bins from $0 < z < 2.0$. These observations include $24\ \mu\text{m}$, $70\ \mu\text{m}$, $160\ \mu\text{m}$, $1.4\ \text{GHz}$ and $610\ \text{MHz}$; the stacked fluxes of the *Spitzer* MIPS bands were then used to fit a M51 SED to estimate $L(\text{TIR})$, which we use to compare with our indicator (Figure 6).

The comparison with Lee et al. (2010) and Bourne et al. (2011) shows excellent agreement and indicates that our description of galaxy SEDs appropriately describes the observations out to $z \sim 3$. There is no indication of systematic trends emerging at $z \sim 1$ and $z \sim 2$ where the $11\ \mu\text{m}$ and $7\ \mu\text{m}$ aromatic complexes redshift into the $24\ \mu\text{m}$ band.

4.3. $L(\text{TIR})$ – SFR Relation

Finally, SFRs can be determined by making use of the relationship between $L(\text{TIR})$ and the rest-frame $L(24\ \mu\text{m})$, and subsequently the $L(24\ \mu\text{m})$ and SFR, given by Rieke et al. (2009) with small modifications. The introduction of the stretching factor, which is effectively to re-normalize the SED templates, requires a modification of the relationship between $L(\text{TIR})$ and $L(24\ \mu\text{m})$. The original fit as given in equation A6 of Rieke et al. (2009) is

$$\log L(\text{TIR})_{\text{old}} = 1.445 + 0.945 \log L(24) \quad (6)$$

The new relationship can be derived by re-fitting equation 6 with the stretching factor, S_i , multiplying both $L(\text{TIR})$ and $L(24\ \mu\text{m})$ for each template i . The re-fitted relation is given by

$$\log L(\text{TIR})_{\text{new}} = 1.113 + 0.980 \log L(24) \quad (7)$$

To determine the SFR from $L(24\ \mu\text{m})$, the calibration given by Rieke et al. (2009) remains valid. However, that calibration has a term that corrects for a decrease in $L(24\ \mu\text{m})/L(\text{TIR})$ above $L(\text{TIR}) = 10^{11}\ L_{\odot}$. Since the correction is motivated by an increase of the optical

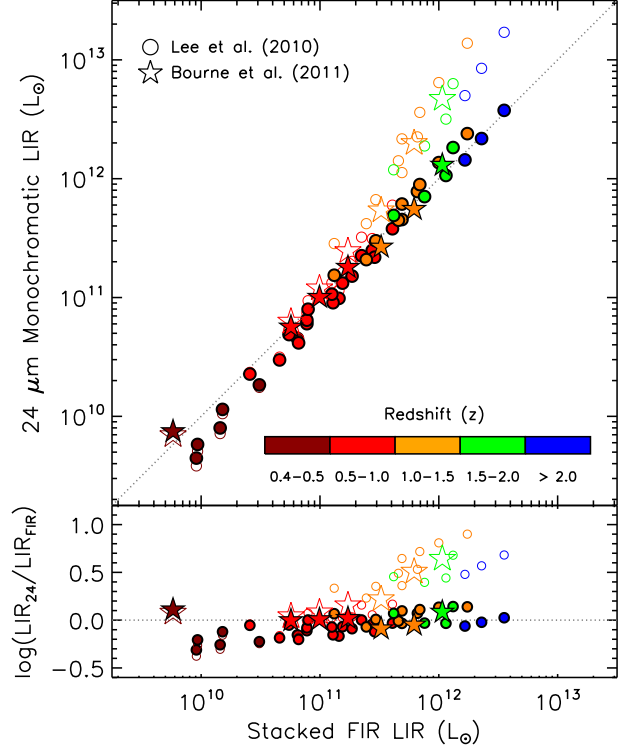


FIG. 6.— Comparison of $L(\text{TIR})$ from our monochromatic $24\ \mu\text{m}$ indicator to $L(\text{TIR})$ measured by stacking far-IR observations. The comparison samples are from Lee et al. (2010) who determined $L(\text{TIR})$ at $0 < z < 3$ by stacking $70\ \mu\text{m}$ and $160\ \mu\text{m}$ observations of over 35,000 COSMOS galaxies, and from Bourne et al. (2011) whose $L(\text{TIR})$ was determined from stacking a broad range of observation from $24\ \mu\text{m}$ to $610\ \text{MHz}$ of 3,172 galaxies at $0 < z < 2$ in the ECDFS-FIDEL sample. Open and filled symbols represent $L(\text{TIR})$ estimates from the Rieke et al. (2009) SED library and this work, respectively. The agreement between estimated and measured $L(\text{TIR})$ also implies that a majority of star-forming galaxies at these redshift resides in the “main sequence” of star-forming galaxies.

depth at high $L(\text{TIR})$ that prevents the mid-IR emission from escaping, the threshold at which optical depth becomes significant depends directly on the geometry of the galaxy. In the same way that the extended structure of the galaxy affects the IR-emitting environment, the optical depth will consequently be lower for a given $L(\text{TIR})$ and the luminosity threshold where the optical depth should apply has to be scaled up by a stretching factor as well. The S_i corresponding to the original threshold is a factor of 3.3, yielding a luminosity threshold of $3.3 \times 10^{11}\ L_{\odot}$. This is equivalent to $L(24\ \mu\text{m})$ of $4.1 \times 10^{10}\ L_{\odot}$. Therefore the relationship between SFR and $L(24\ \mu\text{m})$ is given by

$$\text{SFR}(\text{M}_{\odot}\ \text{yr}^{-1}) = 7.8 \times 10^{-10} L(24\ \mu\text{m}, L_{\odot})$$

for $5 \times 10^9\ L_{\odot} \leq L(\text{TIR}) \leq 3.3 \times 10^{11}\ L_{\odot}$ or $6 \times 10^8\ L_{\odot} \leq L(24\ \mu\text{m}) \leq 4.1 \times 10^{10}\ L_{\odot}$. For $L(\text{TIR}) > 3.3 \times 10^{11}\ L_{\odot}$ or $L(24\ \mu\text{m}) > 4.1 \times 10^{10}\ L_{\odot}$,

$$\text{SFR}(\text{M}_{\odot}\ \text{yr}^{-1}) = 7.8 \times 10^{-10} L(24\ \mu\text{m}, L_{\odot}) \times [2.41 \times 10^{-11} L(24\ \mu\text{m}, L_{\odot})]^{0.048} \quad (8)$$

This calibration is based on that of Kennicutt (1998) but with the Kroupa (2002) IMF, which yields SFRs a factor of 0.66 of those assuming the Salpeter (1955) IMF. A library of IDL routines for the $L(\text{TIR})$ and SFR indicator is available at our website¹. These relations apply at $z \gtrsim 0.3$; within the local volume the $L(\text{TIR})$ and SFR relations given by Rieke et al. (2009) should be used.

5. DISCUSSION

Here we discuss the validity of using $24\ \mu\text{m}$ observation at $0 < z < 3$ to derive $L(\text{TIR})$ and SFR. At these redshifts, this is equivalent to providing justifications that the rest-frame $6 - 24\ \mu\text{m}$ luminosity that encompasses aromatic emissions can be used to estimate $L(\text{TIR})$. We will also discuss the implications of our $L(\text{TIR})$ indicator in light of the test results in Section 4.2.

5.1. Validity of the Aromatic Emission as a $L(\text{TIR})$ and SFR Indicator

Our indicator utilizes the luminosity from observations that correspond to rest-frame wavelengths of $24\ \mu\text{m}$ to $6\ \mu\text{m}$ at $z = 0$ to 3 . This necessitates an investigation into the validity of using the mid-IR-dominating aromatic emission as a tracer for $L(\text{TIR})$. We discuss two major factors affecting the aromatic feature strength: the metallicity dependence and the presence of AGN.

The correlation of the aromatic luminosity to $L(\text{TIR})$ was studied by Rigopoulou et al. (1999), Roussel et al. (2001) and Elbaz et al. (2002) using *ISO*; later by Wu et al. (2005) with *Spitzer*; and recently by Elbaz et al. (2011) with *Herschel*. Calzetti et al. (2007) used the SINGS sample to show that the scatter and the non-linearity of the relationship between the extinction-corrected $8\ \mu\text{m}$ luminosity and the extinction-corrected $\text{Pa}\alpha$ luminosity (which is a good tracer for SFR) is unsatisfactorily large for the former to serve as a SFR indicator. However, their Figure 10 suggests that the largest source of scatter is due to the metallicity differences among the subsamples. For high-metallicity systems ($Z > 1/3\ Z_{\odot}$, which is equivalent to $12 + \log(\text{O}/\text{H}) \gtrsim 8.2$), Calzetti (2010b) reports that the stellar-continuum-subtracted aromatic emission shows a good correlation with the SFR. Furthermore, Engelbracht et al. (2008) and Smith et al. (2007) found that the ratio of aromatic luminosity to $L(\text{TIR})$ does not vary significantly at metallicity $\gtrsim 1/3\ Z_{\odot}$.

Smith et al. (2007) found that AGN can significantly suppress the aromatic emission (see also, Moorwood 1986; Roche et al. 1991; Genzel et al. 1998). The suppression of aromatic luminosity is shown in Figure 7 (left) based on the total aromatic luminosities measured by Smith et al. (2007) and a metallicity measurement from Moustakas et al. (2010). AGN, however, do not affect the aromatic emission of the entire host galaxy. Diamond-Stanic & Rieke (2010) use *Spitzer* IRS to compare nuclear and non-nuclear spectra of nearby Seyfert galaxies and found that the aromatic features in the nuclear spectra are clearly suppressed while the aromatic emission is of normal strength in the outer disk. Therefore, with regard to using aromatic emission to trace $L(\text{TIR})$: (1) the aromatic suppression effect due to AGN

is likely limited to the nuclear region and aromatic emission arising from the rest of the galaxy should still provide a good tracer of the SFR; and (2) the longer wavelength emission such as the $11.3\ \mu\text{m}$ aromatic emission complex, which the $24\ \mu\text{m}$ observation probes at $z \sim 1$, could still serve as a SFR indicator despite the presence of low-luminosity AGN (Diamond-Stanic & Rieke 2010).

Galaxies at $z \sim 2$ have on average 0.3-dex lower metallicity than local galaxies (Erb et al. 2006). Therefore, galaxies more massive than $3 \times 10^9\ M_{\odot}$ should be sufficiently metal rich ($> 1/3\ Z_{\odot}$) that the $L(\text{TIR})$ /aromatic calibration is valid. If we consider the ratio of aromatic-luminosity-to- $L(\text{TIR})$ as a function of metallicity in the left panel of Figure 7 within the range of metallicity expected at high redshift, the scatter of the relationship between aromatic luminosity and $L(\text{TIR})$ is in fact about 0.1-dex in the non-Seyfert/LINER sample. This suggests aromatic luminosity to be a good indicator for $L(\text{TIR})$ at high redshift given that an effort is made to exclude AGN from the sample (such as the AGN exclusion criteria employed in tests in Section 4.2).

We further test the validity of aromatic emission (e.g. $8\ \mu\text{m}$ rest-frame observation) as a measure of $L(\text{TIR})$ in a sample of HII-dominated galaxies with moderate to high metallicity in the right panel of Figure 7. In this Figure, the $8\ \mu\text{m}$ observations are from *Spitzer* and the $L(\text{TIR})$ estimates are based on the *IRAS* all-sky survey using 6 , 12 , 25 , and $60\ \mu\text{m}$ observations (Sanders et al. 2003). This sample is chosen such that it mimics the population of star-forming galaxies expected at high redshift: high-metallicity normal star-forming galaxies without AGN. The scatter of the relationship between $L(8\ \mu\text{m})$ and $L(\text{TIR})$ in Figure 7 is 0.14-dex with the ratio $L(\text{TIR})/L(8\ \mu\text{m})$ of 4.3 ± 1.6 . Elbaz et al. (2011) report a similar ratio measurement locally ($L(\text{TIR})/L(8\ \mu\text{m}) = 4.8^{+6.4}_{-1.7}$) and also show that the ratio is universal for high-redshift galaxies in GOODS-*Herschel*, further reinforcing the applicability of aromatic emission as an $L(\text{TIR})$ and SFR indicator.

5.2. The Eddington Luminosity of ULIRGs

It has been suggested that local ULIRGs are optically thick to mid-IR photons and radiation pressure may play a role in limiting their maximum luminosity (Thompson et al. 2005; Younger et al. 2008; Thompson 2009). If the degree of compactness is assumed to be similar for both the local and high-redshift ULIRGs, an obvious problem would arise that the IR emission of high-redshift ULIRGs with $L(\text{TIR})$ commonly found far above their local counterparts would exceed the Eddington luminosity. Our results ease the concerns about the Eddington limit of ULIRGs at high redshift for two reasons. First, galaxies at higher $L(\text{TIR})$ are affected by the mid-IR excess to a greater extent. Our new indicator would therefore lower the $L(\text{TIR})$ estimates especially for high-luminosity galaxies. To test the effects of $L(\text{TIR})$ reduction to the luminosity functions of galaxies, we construct a set of IR LFs of $24\ \mu\text{m}$ sources at $0 < z < 2.5$ using the $24\ \mu\text{m}$ observations from COSMOS (e.g. Sanders et al. 2007) and find that the bright-end of the LFs in all redshift bins are below $L(\text{TIR})$ of $\sim 10^{13}\ L_{\odot}$ (quantitatively, galaxies with $L(\text{TIR})$ above $10^{13}\ L_{\odot}$ are rarer than $10^{-6}/\text{Mpc}^3/\text{dex}$ in all redshift

¹ <http://ircamera.as.arizona.edu/rujopakarn2011>

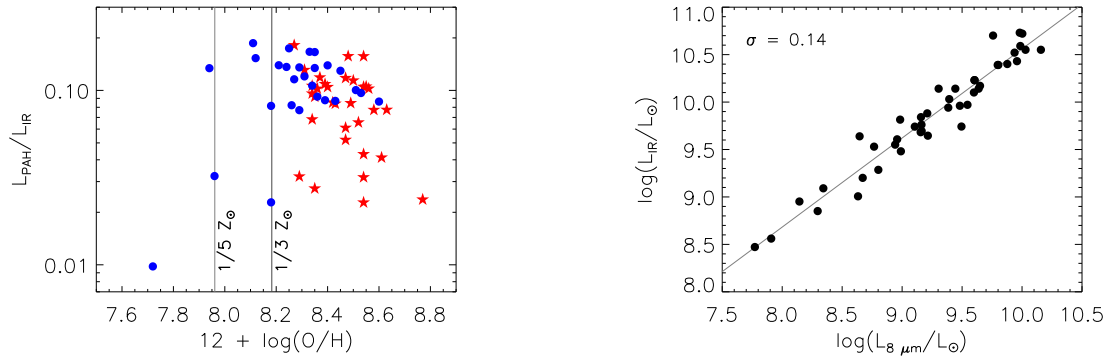


FIG. 7.— (Left) The sources of scatter in using aromatic emissions (e.g. PAH) to predict $L(\text{TIR})$ and SFR are primarily the metallicity dependence and the presence of AGN. Blue dots and red stars show the ratios of aromatic luminosity to $L(\text{TIR})$ as a function of metallicity for HII and AGN dominated local galaxies, respectively (Smith et al. 2007). For HII-dominated galaxies with metallicity greater than $1/3 Z_{\odot}$ (solid vertical line), which is similar to the environment of high-redshift star-forming galaxies, the correlation of aromatic luminosity, L_{PAH} , and $L(\text{TIR})$ has a ~ 0.1 -dex scatter, suggesting that aromatic emission could serve as a good $L(\text{TIR})$ and SFR indicators at high redshift. (Right) The correlation between the rest-frame $L(8 \mu\text{m})$ and $L(\text{TIR})$ for local star-forming galaxies that are dominated by HII-emission and have high metallicity, similar to those expected at high redshift, has a scatter of 0.14-dex. The small scatter underlines the potential of using aromatic emission as a $L(\text{TIR})$ and SFR indicator.

bins), which suggests that the maximum $L(\text{TIR})$ of star-forming galaxies is in general less than $10^{13} L_{\odot}$. Second, the success of the corrections for the size evolution described in Rujopakarn et al. (2011) as well as this work to account for the general IR SED evolution indicate that the great majority of high-redshift IR galaxies are physically extended, which lowers the optical depth of the galaxy. Both the lower $L(\text{TIR})$ and extended structure imply that high-redshift ULIRGs are emitting below the Eddington limit and that the maximum $L(\text{TIR})$ of these galaxies is not governed by radiation pressure.

5.3. Modes of Star Formation

In deriving the stretching factors from the local $\Sigma_{L(\text{TIR})}$ - $L(\text{TIR})$ relation to the main sequence relation, there is an implicit assumption that there are two distinct relations: one for local galaxies with $L(\text{TIR}) > 10^{11} L_{\odot}$ generally from compact nuclear regions (starburst mode) and another for the main sequence galaxies. This is motivated by the fact that local U/LIRGs are rare objects found only by large-volume surveys such as the *IRAS* all-sky survey, and that most of them are interacting systems with compact central starbursts. Beyond the local universe, other surveys do not encompass enough volume to find similar systems in large numbers.

At intermediate and high redshift, the precise fraction of galaxies that form stars in starburst mode remains a subject of controversy. A tracer for starburst mode star-formation is the galaxy merger fraction, which can be estimated from morphological studies. Lotz et al. (2008) report a relatively constant major merger (i.e., mass ratio $> 1 : 3$) fraction of $10\% \pm 2\%$ for all galaxies in their sample at $0.2 < z < 1.2$ and $\sim 15\%$ for U/LIRGs. Shi et al. (2009) find that the fraction of galaxies exhibiting asymmetric morphologies in the same redshift range is $20\% - 30\%$ and as many as $\sim 50\%$ for LIRGs. The Lotz et al. (2008) figures represent a conservative estimate by limiting mergers to major mergers while the Shi et al. (2009) provides an upper limit, since not all asymmetric galaxies are mergers. For ULIRG and LIRG populations at $z < 1$, Kartaltepe et al. (2010) find that the merger fractions are $\sim 50\% - 80\%$ and $\sim 25\% - 40\%$,

respectively. However, morphological studies are increasingly compromised by the limited angular resolution and surface brightness sensitivity at higher redshifts. More importantly, disturbed morphologies found at high redshift are not necessary a result of mergers but could also be due to clumpy or asymmetric star-formation in gas-rich environments such as those recently observed by Swinbank et al. (2010b) and Hailey-Dunsheath et al. (2010) as well as those emerging in cosmological simulations by Agertz et al. (2009) and Davé et al. (2010). The range of $15\% - 50\%$ can be taken as a broad constraint on the fraction of systems undergoing interaction up to $z \sim 1.2$, depending on how merger is defined. These merger fraction estimates imply that the interaction-induced starburst mode is a significant yet unlikely a dominant mode of star formation at intermediate and high redshift.

On the other hand, many recent observations support the main sequence picture of star-forming galaxies at intermediate and high redshift. The supporting evidence includes the finding that high-redshift star-forming galaxies lack evidence for interactions and that these galaxies have extended star-forming regions, contradicting the picture of compact starbursts. Targett et al. (2010) find that 95% of optical morphologies of radio/sub-mm galaxies at $z \sim 2$ are consistent with normal disk galaxies, well described by axi-symmetric disk-like models. Similarly, Yuma et al. (2011) find that the UV morphology of BzK galaxies at $z \sim 2$ that have a single component also shows consistent Sérsic indices with those of normal disks. Extended physical sizes of high-redshift star-forming galaxies, U/LIRGs, and submillimeter galaxies have been reported extensively in the literature (Chapman et al. 2004; Muxlow et al. 2005; Biggs & Ivison 2008; Bothwell et al. 2010; Casey et al. 2009; Iono et al. 2009; Lehnert et al. 2009; Carilli et al. 2010; Swinbank et al. 2010a; Tacconi et al. 2010; Younger et al. 2010). In this study, the assumption that star-forming galaxies lie on the main sequence allows assignment of their SED template based on $\Sigma_{L(\text{TIR})}$ that successfully predicts high redshift galaxy SEDs, and subsequently, their $L(\text{TIR})$. From various tests of

the $L(\text{TIR})$ indicator from this work against $L(\text{TIR})$ estimated from far-IR SED fitting for a broad range of galaxies out to $z \sim 3$ in Section 4.2, the good agreement and small scatter support the initial assumption that a majority of star-forming galaxies beyond the local universe reside in the main sequence of star-forming galaxies.

6. CONCLUSIONS

The use of monochromatic mid-IR indicators (such as $24\ \mu\text{m}$ photometry) has previously been affected by the differences between the structure of local U/LIRGs, upon which the SED templates were constructed, and the galaxies in the cosmological surveys being studied. Starbursts in the local U/LIRGs are almost invariably interaction-induced and very compact, while U/LIRGs at high-redshift are much more extended. High-redshift U/LIRGs typically have surface areas $\sim 100\times$ larger than their local counterparts. The resulting larger surface area of the photodissociation regions harboring aromatic emission leads to stronger aromatic features at high-redshift mimicking an evolution in aromatic strength as a function of redshift. The ultimate implication of this morphological difference is that monochromatic mid-IR observations, which at $z > 1$ probe the aromatic-dominated SED region, will overpredict $L(\text{TIR})$ and SFR compared to far-IR measurements if the relationship of local SED templates to $L(\text{TIR})$ is assumed for k -correction.

Following the Rujopakarn et al. (2011) result that $\Sigma_{L(\text{TIR})}$ can serve as a good predictor for the appropriate SED of star-forming galaxies, we determine a new $24\ \mu\text{m}$ monochromatic $L(\text{TIR})$ and SFR indicator valid for star-forming galaxies at redshift $0.3 < z < 3$ (the Rieke et al. (2009) indicator should be used at $z < 0.3$).

Two relationships are derived. A preliminary result is based on the formal fit to the $L(\text{TIR})$ - Σ_{SFR} relation of the local galaxies. We refine this fit with a small adjustment to improve the agreement to the FIR measurements. The fact that the use of $\Sigma_{L(\text{TIR})}$ as an indicator of SED shape allows us to derive $L(\text{TIR})$ highly consistently with the FIR measurements (within 0.2-dex) confirms the Rujopakarn et al. (2011) result that $\Sigma_{L(\text{TIR})}$ is indeed the dominant factor affecting the SED shapes of star-forming galaxies. However, the need for a small modification of the calibration suggests $\Sigma_{L(\text{TIR})}$ may not be the sole parameter affecting the SED, or that there is a room for improvement in the sample of local star formation-dominated U/LIRGs to better constrain the local $L(\text{TIR})$ - $\Sigma_{L(\text{TIR})}$ relation.

For estimating $L(\text{TIR})$ consistent with the FIR $L(\text{TIR})$ measurements (from, e.g., *Herschel*) within 0.1-dex using monochromatic $24\ \mu\text{m}$ observations, the use of the latter calibration (i.e. apply equation 5 with the $A^*(z)$ and $B^*(z)$ coefficients provided in Table 2) is encouraged. Given the $L(\text{TIR})$, the $L(24\ \mu\text{m})$ and SFR can then be determined by equations 7 and 8, respectively. A monochromatic $24\ \mu\text{m}$ indicator will facilitate the study of the SFR of galaxies at high redshifts, particularly at $z \sim 2$ where the strong $7.7\ \mu\text{m}$ aromatic emission complex redshifts into the *Spitzer* $24\ \mu\text{m}$ band as well as with the future 21 and $25.5\ \mu\text{m}$ bands of the Mid-Infrared Instrument on *JWST*.

We thank Daniel Eisenstein for insightful discussions and J. D. Smith for the $L_{\text{PAH}}/L(\text{TIR})$ data. This work is supported by contract 1255094 from Caltech/JPL to the University of Arizona. WR gratefully acknowledges the support from the Thai Government Scholarship.

REFERENCES

- Agertz, O., Teyssier, R., & Moore, B. 2009, *MNRAS*, 397, L64
 Armus, L., et al. 2007, *ApJ*, 656, 148
 Biggs, A. D., & Ivison, R. J. 2008, *MNRAS*, 385, 893
 Bothwell, M. S., et al. 2010, *MNRAS*, 525
 Bourne, N., Dunne, L., Ivison, R. J., Maddox, S. J., Dickinson, M., & Frayer, D. T. 2011, *MNRAS*, 410, 1155
 Buat, V., et al. 2007, *ApJS*, 173, 404
 Calzetti, D., et al. 2007, *ApJ*, 666, 870
 Calzetti, D., et al. 2010, *ApJ*, 714, 1256
 Calzetti, D. 2010, arXiv:1010.4996
 Carilli, C. L., et al. 2010, *ApJ*, 714, 1407
 Casey, C. M., et al. 2009, *MNRAS*, 399, 121
 Chakrabarti, S., & McKee, C. F. 2005, *ApJ*, 631, 792
 Chial, P., Flores, H., Guiderdoni, B., Elbaz, D., Hammer, F., & Vigroux, L. 2007, *A&A*, 462, 81
 Chapman, S. C., Smail, I., Windhorst, R., Muxlow, T., & Ivison, R. J. 2004, *ApJ*, 611, 732
 Chary, R., & Elbaz, D. 2001, *ApJ*, 556, 562
 Dale, D. A. & Helou, G. 2002, *ApJ*, 576, 159
 Daddi, E., et al. 2010, *ApJ*, 714, 118
 Davé, R., Finlator, K., Oppenheimer, B. D., Fardal, M., Katz, N., Keres, D., & Weinberg, D. H. 2010, *MNRAS*, 404, 1355
 Diamond-Stanic, A. M., & Rieke, G. H. 2010, *ApJ*, 724, 140
 Dole, H., et al. 2004, *ApJS*, 154, 93
 Dole, H., et al. 2006, *A&A*, 451, 417
 Dye, S., et al. 2009, *ApJ*, 703, 285
 Eales, S., et al. 2009, *ApJ*, 707, 1779
 Egami, E., et al. 2010, *A&A*, 518, L12
 Elbaz, D., Cesarsky, C. J., Chial, P., Aussel, H., Franceschini, A., Fadda, D., & Chary, R. R. 2002, *A&A*, 384, 848
 Elbaz, D., et al. 2010, *A&A*, 518, L29
 Elbaz, D., et al. 2011, arXiv:1105.2537
 Engelbracht, C. W., Rieke, G. H., Gordon, K. D., Smith, J.-D. T., Werner, M. W., Moustakas, J., Willmer, C. N. A., & Vanz, L. 2008, *ApJ*, 678, 804
 Erb, D. K., Shapley, A. E., Pettini, M., Steidel, C. C., Reddy, N. A., & Adelberger, K. L. 2006, *ApJ*, 644, 813
 Farrah, D., et al. 2008, *ApJ*, 677, 957
 Genzel, R., et al. 1998, *ApJ*, 498, 579
 Genzel, R., et al. 2010, *MNRAS*, 407, 2091
 Hopkins, A. M., & Beacom, J. F. 2006, *ApJ*, 651, 142
 Hailey-Dunsheath, S., Nikola, T., Stacey, G. J., Oberst, T. E., Parshley, S. C., Benford, D. J., Staguhn, J. G., & Tucker, C. E. 2010, *ApJ*, 714, L162
 Iono, D., et al. 2009, *ApJ*, 695, 1537
 Johansson, D., et al. 2010, *A&A*, 514, A77
 Kartaltepe, J. S., et al. 2010, *ApJ*, 709, 572
 Kartaltepe, J. S., et al. 2010, *ApJ*, 721, 98
 Kennicutt, R. C. 1998, *ARA&A*, 36, 189
 Kennicutt, R. C., et al. 2009, *ApJ*, 703, 1672
 Kroupa, P. 2002, *Science*, 295, 82
 Lagache, G., Dole, H., & Puget, J.-L. 2003, *MNRAS*, 338, 555
 Lee, N., et al. 2010, *ApJ*, 717, 175
 Le Floc'h, E., et al. 2005, *ApJ*, 632, 169
 Lehnert, M. D., Nesvadba, N. P. H., Tiran, L. L., Matteo, P. D., van Driel, W., Douglas, L. S., Chemin, L., & Bournaud, F. 2009, *ApJ*, 699, 1660
 Lotz, J. M., et al. 2008, *ApJ*, 672, 177
 Magnelli, B., Elbaz, D., Chary, R. R., Dickinson, M., Le Borgne, D., Frayer, D. T., & Willmer, C. N. A. 2009, *A&A*, 496, 57
 Moorwood, A. F. M. 1986, *A&A*, 166, 4
 Moustakas, J., Kennicutt, R. C., Jr., Tremonti, C. A., Dale, D. A., Smith, J.-D. T., & Calzetti, D. 2010, *ApJS*, 190, 233
 Muxlow, T. W. B., et al. 2005, *MNRAS*, 358, 1159

- Muzzin, A., van Dokkum, P., Kriek, M., Labbé, I., Cury, I., Marchesini, D., & Franx, M. 2010, *ApJ*, 725, 7
- Narayanan, D., Cox, T. J., Hayward, C., & Hernquist, L. 2010, arXiv:1005.3020
- Noeske, K. G., et al. 2007, *ApJ*, 660, L47
- Nordon, R., et al. 2010, *A&A*, 518, L24
- Pascale, E., et al. 2008, *ApJ*, 681, 400
- Pope, A., et al. 2006, *MNRAS*, 370, 1185
- Pérez-González, P. G., et al. 2005, *ApJ*, 630, 82
- Reddy, N. A., Erb, D. K., Pettini, M., Steidel, C. C., & Shapley, A. E. 2010, *ApJ*, 712, 1070
- Rex, M., et al. 2010, *A&A*, 518, L13
- Rieke, G. H., Alonso-Herrero, A., Weiner, B. J., Pérez-González, P. G., Blaylock, M., Donley, J. L., & Marcillac, D. 2009, *ApJ*, 692, 556
- Rigby, J. R., et al. 2008, *ApJ*, 675, 262
- Rigopoulou, D., Spoon, H. W. W., Genzel, R., Lutz, D., Moorwood, A. F. M., & Tran, Q. D. 1999, *AJ*, 118, 2625
- Roche, P. F., Aitken, D. K., Smith, C. H., & Ward, M. J. 1991, *MNRAS*, 248, 606
- Roussel, H., Sauvage, M., Vigroux, L., & Bosma, A. 2001, *A&A*, 372, 427
- Royer, P., et al. 2010, *A&A*, 518, L145
- Rujopakarn, W., Rieke, G. H., Eisenstein, D. J., & Juneau, S. 2011, *ApJ*, 726, 93
- Salpeter, E. E. 1955, *ApJ*, 121, 161
- Sanders, D. B., & Mirabel, I. F. 1996, *ARA&A*, 34, 749
- Sanders, D. B., Mazzarella, J. M., Kim, D.-C., Surace, J. A., & Soifer, B. T. 2003, *AJ*, 126, 1607
- Sanders, D. B., et al. 2007, *ApJS*, 172, 86
- Shi, Y., Rieke, G., Lotz, J., & Perez-Gonzalez, P. G. 2009, *ApJ*, 697, 1764
- Siebenmorgen, R., & Krügel, E. 2007, *A&A*, 461, 445
- Smith, J. D. T., et al. 2007, *ApJ*, 656, 770
- Soifer, B. T., Sanders, D. B., Madore, B. F., Neugebauer, G., Danielson, G. E., Elias, J. H., Lonsdale, C. J., & Rice, W. L. 1987, *ApJ*, 320, 238
- Swinbank, M., et al. 2010a, arXiv:1002.2518
- Swinbank, A. M., et al. 2010, *Nature*, 464, 733
- Symeonidis, M., Page, M. J., Seymour, N., Dwelly, T., Coppin, K., McHardy, I., Rieke, G. H., & Huynh, M. 2009, *MNRAS*, 397, 1728
- Takagi, T., et al. 2010, *A&A*, 514, A5
- Tacconi, L. J., et al. 2010, *Nature*, 463, 781
- Targett, T. A., Dunlop, J. S., McLure, R. J., Best, P. N., Cirasuolo, M., & Almaini, O. 2010, arXiv:1005.5176
- Thompson, T. A., Quataert, E., & Murray, N. 2005, *ApJ*, 630, 167
- Thompson, T. A. 2009, *Astronomical Society of the Pacific Conference Series*, 408, 128
- Tielens, A. G. G. M. 2008, *ARA&A*, 46, 289
- Truch, M. D. P., et al. 2009, *ApJ*, 707, 1723
- Veilleux, S., Kim, D.-C., & Sanders, D. B. 2002, *ApJS*, 143, 315
- Wilson, G. W., et al. 2008, *MNRAS*, 390, 1061
- Wu, H., Cao, C., Hao, C.-N., Liu, F.-S., Wang, J.-L., Xia, X.-Y., Deng, Z.-G., & Young, C. K.-S. 2005, *ApJ*, 632, L79
- Younger, J. D., et al. 2008, *ApJ*, 688, 59
- Younger, J. D., et al. 2010, *MNRAS*, 984
- Yuma, S., Ohta, K., Yabe, K., Kajisawa, M., & Ichikawa, T. 2011, arXiv:1105.2598